Mechanistic Interplay between Light Switching and Guest Binding in Photochromic [Pd 2 Dithienylethene 4] Coordination Cages

JACS
JOURNAL OF THE AMERICAN CHEMICAL SOCIETY
Article
Cite This: J. Am. Chem. Soc. 2019, 141, 2097−2103
pubs.acs.org/JACS

Mechanistic Interplay between Light Switching and Guest Binding in Photochromic [Pd_2Dithienylethene$_4$] Coordination Cages

Ru-Jin Li,[†] Julian. J. Holstein,[†] Wolf G. Hiller,[†] Joakim Andréasson,[§] and Guido H. Clever*[,†]

[†]Faculty of Chemistry and Chemical Biology, TU Dortmund University, Otto-Hahn-Straße 6, 44227 Dortmund, Germany
[§]Department of Chemistry and Chemical Engineering, Chalmers University of Technology, 41296, Göteborg, Sweden

Supporting Information

ABSTRACT: Photochromic [$Pd_2\mathbf{L}_4$] coordination cages based on dithienylethene (DTE) ligands **L** allow triggering guest uptake and release by irradiation with light of different wavelengths. The process involves four consecutive electrocyclic reactions to convert all chromophores between their open and closed photoisomeric forms. So far, guest affinity of the fully switched species was elucidated, but mechanistic details concerning the intermediate steps remained elusive. Now, a new member of the DTE cage family allows unprecedented insight into the interplay between photoisomerization steps and guest location inside/outside the cavity. Therefore, the intrinsic chirality of the DTE backbones was used as reporter for monitoring the fate of a chiral guest. In its "open" photoisomeric form (*o*-**L**, [Pd_2(*o*-**L**)$_4$] = *o*-**C**), the C_2-symmetric DTE chromophore quickly converts between energetically degenerate *P* and *M* helical conformations. After binding homochiral 1*R*-(−) or 1*S*-(+) camphor sulfonate (*R*-CSA or *S*-CSA), guest-to-host chirality transfer was observed via a circular dichroism (CD) signal for the cage-centered absorption. Irradiating the *R*/*S*-CSA@*o*-**C** host−guest complexes at 313 nm produced configurationally stable "closed" photoisomers, thus locking the induced chirality with an enantiomeric excess close to 25%. This value (corresponding to chiral induction for one out of four ligands), together with DOSY NMR, ion mobility mass spectrometry, and X-ray structure results, shows that closure of the first photoswitch is sufficient to expel the guest from the cavity.

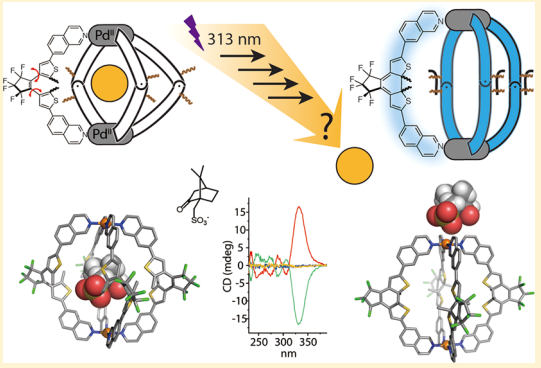

INTRODUCTION

Stimuli-responsive supramolecular systems raise significant research interest since they allow the understanding and mimicking of dynamic biological structures, realize molecular machines, and lead to new materials.[1] Light is the trigger of choice due to its traceless character and facile application.[2] Symmetric, self-assembled systems with light-triggered function, e.g., guest binding and release, are likely to contain more than one chromophore. Since a concerted isomerization of all switches is extremely improbably under conventional irradiation conditions, the question arises at which point during a stepwise photoswitching process do key structural changes take place. Without further insight into this phenomenon, the understanding and rational development of supramolecular hosts and machines containing more than one photoswitch lacks important information. However, meaningful insight into processes occurring during the continuous irradiation of a photoswitchable system is difficult to obtain since spectroscopic online monitoring (e.g., by NMR) suffers from signal convolution due to nonsynchronized switching events. In addition, vastly different time scales of the basic photoreaction, its supramolecular implication, and the spectroscopic method pose complications to such experiments. Here, we make use of a guest-to-host chirality transfer phenomenon, with the photoswitch acting as an internal reporter group, to elucidate the temporal relationship between host photoisomerization and guest binding.

The propagation of chirality is a central feature in the biosynthesis of natural products, in man-made homogeneous catalysis and recent developments in polymer sciences.[3] Besides the direct influence of covalently bound chiral substructures or auxiliaries, the transfer of stereochemical information through noncovalent contacts is a major pathway.[4] In supramolecular chemistry, chirality has been introduced into self-assembled cavities via chiral backbones, metal centers, covalently bound moieties, and emerging as a topological effect.[5] In certain cases, systems were even found to keep a stereochemical memory after the chiral building block has been replaced.[6] Also noncovalent implementation of chiral information has been realized over the past decades, examples including the template-directed formation of dissymmetric, hydrogen-bonded capsules, reported by Rebek,[7] and a complete resolution of chiral M_4L_6 tetrahedra assembled in the presence of a chiral guest, as shown by Raymond et al.[8]

Received: November 4, 2018
Published: January 8, 2019

DOI: 10.1021/jacs.8b11872
J. Am. Chem. Soc. 2019, 141, 2097−2103

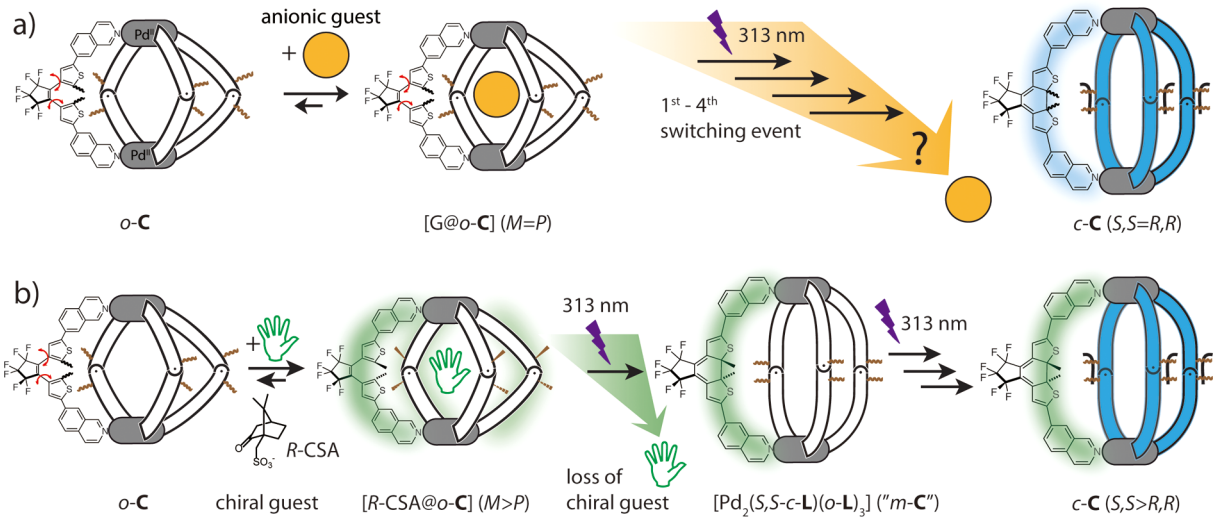

Figure 1. (a) Open-cage *o*-**C** based on four DTE photoswitches is able to bind anionic guests and can be transformed into a diastereomeric mixture of closed cages *c*-**C** by irradiation with UV light (313 nm; back reaction at 617 nm).[15a] This leads to excretion of the encapsulated guest molecule, but it was previously not known when this occurs during the stepwise photoconversion. (b) Encapsulation of a chiral guest (*R*-CSA, *S*-CSA, or *S*-CSA-Br) into *o*-**C** induces *P* or *M* helical chirality of the DTE chromophores. Irradiation at 313 nm locks the induced chirality onto the structure of the first cyclized ligand, followed by a change of overall cage shape and ejection of the guest. The remaining three ligands are then photoswitched to give cage *c*-**C** without further induced stereoselectivity.

Recently, intrinsically chiral dithienylethene (DTE) chromophores[9] were recognized to be attractive reporter groups for the quantification of noncovalent chirality transfer.[10] The basis for this capability is the transition between rapid epimerization shown by their open-form photoisomers and fixed stereochemistry present in the closed-form isomers. For example, van Esch and Feringa used DTE-based gels to demonstrate optical transcription of supramolecular into molecular chirality.[11] Andréasson achieved noncovalent binding of cationic DTE derivatives to DNA, followed by enantioselective photoswitching.[12]

Here, we demonstrate that chiral guest-to-host induction can yield valuable information about the guest location within the framework of a lantern-shaped $[Pd_2L_4]$ coordination cage,[13,14] which represents a new member of our recently introduced family of photochromic DTE cages[15] with a stimuli-responsive host–guest chemistry.[2a,16] In contrast to previously reported systems, chiral guests are not required as templates for cage formation, thus allowing a comparative study of hosts in the presence and absence of guests. Circular dichroism (CD), density functional theory (DFT), and chiral HPLC results allowed us to relate the absolute configurations of guest and host and calculate the enantiomeric excess of isolated DTE backbones as a function of temperature during the photochemical fixation process. Resulting values, together with DOSY NMR and trapped ion mobility mass spectrometry, reveal that the first photoisomerization event triggers guest release in this system.

RESULTS AND DISCUSSION

Ligand and Cage Synthesis. Following our previously reported protocols,[15] ligand *o*-**L** was synthesized by a Suzuki cross-coupling reaction of perfluoro-1,2-bis(2-iodo-5-methylthien-4-yl)cyclopentene and 2 equiv of isoquinolin-7-ylboronic acid. By combining a 2:1 mixture of *o*-**L** with $[Pd(CH_3CN)_4](BF_4)_2$ in CD_3CN at 70 °C for 3 h, the light yellow cage $[Pd_2(o\text{-}L)_4](BF_4)_4$ (*o*-**C**) was formed quantitatively, as confirmed by ^1H NMR spectroscopy, high-resolution ESI mass spectrometry (Figure 2), and single-crystal X-ray diffraction analysis (Figure 3a). Upon conversion of ligand

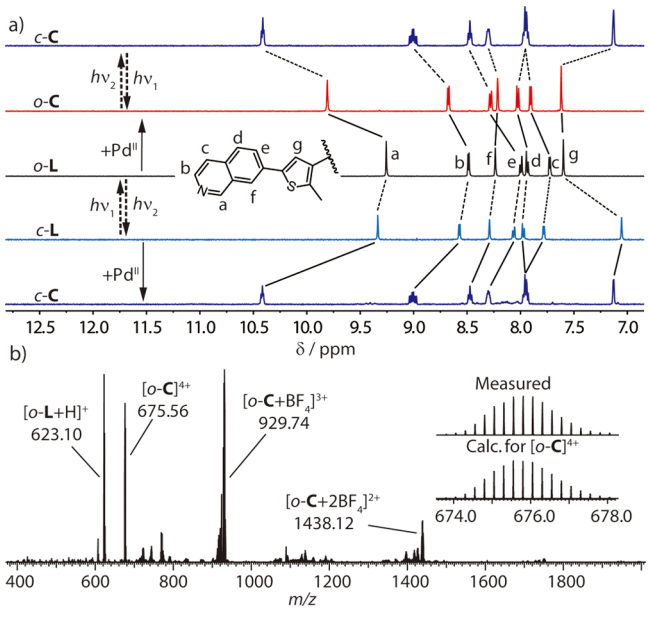

Figure 2. (a) ^1H NMR spectra (500 MHz, CD_3CN, 298 K) of ligands *o*-**L**, *c*-**L** and cages *o*-**C**, *c*-**C**; (b) ESI-MS spectrum of *o*-**C** with an isotope pattern of $[o\text{-}C]^{4+}$ shown in the inset.

into cage, the ^1H NMR signals of the isoquinolines, in particular protons H_a ($\Delta\delta$ = 0.56 ppm) and H_b ($\Delta\delta$ = 0.20 ppm), sitting close to the coordinating nitrogen atoms, undergo significant downfield shifts (Figure 2a). The ESI mass spectrum displayed a series of species supporting the expected composition with a variable number of BF_4^- counterions ($[o\text{-}C]^{4+}$, $[o\text{-}C+BF_4]^{3+}$, and $[o\text{-}C+2BF_4]^{2+}$). In all cases, experimental isotope patterns were found to be in very good agreement with the calculated distributions (Figure 2b).

DOI: 10.1021/jacs.8b11872
J. Am. Chem. Soc. 2019, 141, 2097–2103

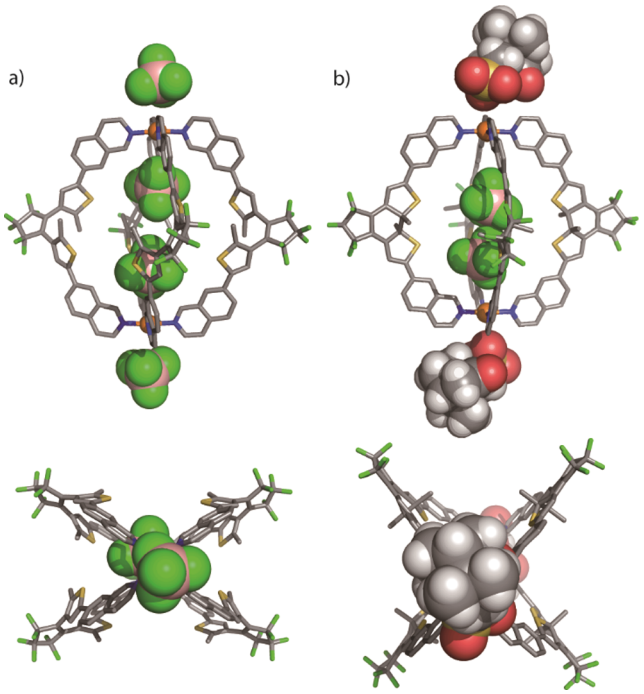

Figure 3. X-ray structures of (a) cage *o*-**C** and (b) *c*-**C** cocrystallized with *R*-CSA (side and top view) showing counteranions/guests inside and outside the cavities. All hydrogen atoms, solvent molecules, and minor disordered components have been omitted (for details see the Supporting Information). In *c*-**C**, all backbone methyl groups are disordered over both possible positions with approximately 50% occupancy (here only one diastereomer is shown; B pink, C gray, N blue, O red, F green, S yellow, Pd orange).

The structure of cage *o*-**C**, possessing all four DTE switches in their open photoisomeric form, was finally proven by X-ray analysis. Therefore, single crystals were obtained by slow vapor diffusion of ethyl ether into an acetonitrile solution of *o*-**C** (Figure 3a). Cage *o*-**C** crystallized with low crystallographic symmetry in the triclinic space group $P\bar{1}$ and features a *cis-PPMM* arrangement of both helical conformers (*M* and *P*) of the DTE backbone within each single cage. As a result, the molecular structure has a mirror plane (containing the Pd_2 axis with Pd···Pd distance = 15.06 Å), leading to a *meso*-arrangement with C_{2h}-symmetry. It has to be noted, however, that in ambient temperature solution, we expect the system to exist as an inseparable and rapidly interconverting mixture of all possible diastereomers, as indicated by the observation of strikingly sharp signals in the ^{1}H NMR spectrum of *o*-**C** (in full accordance with a related DTE cage derivative).[15a]

Photoswitching. Ligand **L** can be reversibly interconverted between its open and photoisomeric closed form by irradiation with UV light (313 nm) and longer wavelength light (617 nm), respectively. Closed-form cage $[Pd_2(c\text{-}\mathbf{L})_4](BF_4)_4$ (*c*-**C**) could be obtained from self-assembly of *c*-**L** and Pd^{II} or directly from open-form cage *o*-**C** by irradiating a CD_3CN solution of the latter compound under 313 nm UV light (Figure 2a and Supporting Information Figure S23). Unlike conformationally flexible ligand *o*-**L**, closed-form isomer *c*-**L** comes in two separable enantiomers. As a result, a maximum of six possible cage stereoisomers of *c*-**C** can form from a racemic mixture of ligand *c*-**L**.[15a] Indeed, both the ^{1}H NMR (Figure 2) and ^{13}C NMR spectra (Supporting Information Figure S18) show a splitting and broadening for all proton and carbon NMR signals due to the diversity of the contained diastereomers. Under strict exclusion of light, we were able to obtain a crystal of cage *c*-**C** suitable for X-ray structure determination (formed in the course of a ^{1}H NMR titration with *S*-CSA). As observed for *o*-**C**, cage *c*-**C** was found to crystallize in the triclinic space group *P*1, however, showing a slightly shorter Pd···Pd distance of 14.67 Å (Figure 3b). Most strikingly, the cage cocrystallized with an *R*-CSA guest molecule situated outside the cage's cavity, in full agreement with the solution results concerning guest binding (see below).

Guest Binding and Chiral Induction. With both open and closed cages in hand, we set out to test whether encapsulation of chiral guests can induce a transfer of chiral information onto the surrounding cage structure. Via ^{1}H NMR titration experiments, we first checked both cage photoisomers for encapsulation of the anionic *R*-CSA *or S*-CSA, respectively. Upon stepwise addition of *R*-CSA into a solution of *o*-**C**, the ^{1}H NMR signal of inward pointing proton H_a was found to broaden and gradually shift downfield until about 1.0 equiv of *R*-CSA had been added. The signal of outward pointing proton H_b, however, did not show any significant shift in this concentration range but started to move after more than 1.0 equiv of guest had been added, thereby indicating encapsulation of one equivalent of chiral guest followed by external association after saturation of the cage interior (Figure 4a and Supporting Information Figure S27). Since titration beyond 1.0 equiv was accompanied by the onset of aggregation (solution turning turbid and formation of precipitates), we were not able to determine binding constants. Furthermore, a DOSY NMR experiment on *R*-CSA@*o*-**C** revealed encapsulation by observing the guest peaks at a similar diffusion constant to the host (log $D \approx -9.7$; Figure S30).

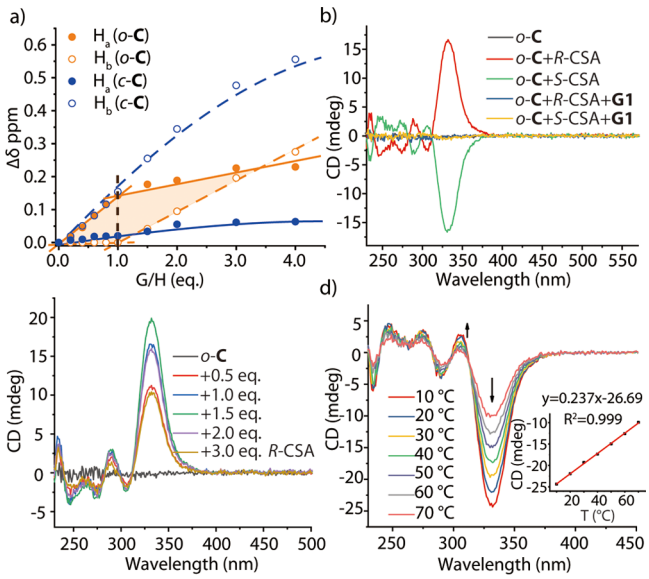

Figure 4. (a) ^{1}H NMR titration plot of *o*-**C** (orange) and *c*-**C** (blue; 1.0 mM, CD_3CN) with *R*-CSA (15 mM, CD_3CN) with relative signal shifts of inward pointing protons H_a (closed circles) and outward H_b (open circles), indicating 1:1 encapsulation for *o*-**C** but unspecific interaction for *c*-**C**; (b) CD spectra of *o*-**C** (0.05 mM, CH_3CN) with and without 1.0 equiv of *R*-CSA or *S*-CSA and after addition of 1.0 equiv of competitor **G1** (as NBu_4 salts in CD_3CN, 15 mM); (c) CD spectra of *o*-**C** with increasing amounts of *R*-CSA; (d) CD spectra of *o*-**C** (0.05 mM, CH_3CN) with 1.5 equiv of *S*-CSA between 10 and 70 °C and $CD_{330\ nm}$ over *T* plot showing a linear relationship (inset).

DOI: 10.1021/jacs.8b11872
J. Am. Chem. Soc. 2019, 141, 2097−2103

In contrast, the titration of closed cage *c*-**C** with *R*-CSA resulted in significant shifting of only outward pointing proton H_b. Inward-pointing signal H_a, however, was observed to undergo almost no shifting but broadening, instead, indicative of unspecific external association favored over uptake inside the cavity (Figure 4a and Supporting Information Figure S27). This assumption was also backed by the obtained X-ray structure, showing cocrystallized guest exclusively outside the cage (Figure 3b). In addition, ion mobility mass spectrometry experiments further confirmed the external interaction of CSA with *c*-**C** (see below).

Next, CD spectra were measured to examine the degree of chirality transfer. As expected, no CD signal was detected for open-form cage *o*-**C**. Addition of 1.0 equiv of *R*- or *S*-CSA, however, led to the occurrence of strong Cotton effects assigned to the ligand chromophore, indicative of a transfer of chiral information from guest to host (Figure 4b). Interestingly, this effect could be reversed by addition of 1.0 equiv of the nonchiral guest benzene-1,4-disulfonate (**G1**), which binds stronger inside the cavity and is able to completely replace monoanionic camphor sulfonate (Figure 4b). The latter was further confirmed by a ^{1}H NMR experiment (Supporting Information Figure S37). Variation of relative guest concentration between 0 and 3.0 equiv reveals that the CD signals pass through a maximum around 1.5 equiv with larger guest amounts leading to aggregation effects that reduce the signal intensity (Figure 4c). We further monitored the CD signal intensity of *o*-**C** containing 1.5 equiv of *S*-CSA as a function of temperature, revealing that increasing temperature leads to decreasing ellipticity, most probably caused by a decreased binding affinity at higher temperatures (Figure 4d).

Like the situation for *o*-**C**, the mixture of closed-form cage *c*-**C** diastereomers did not show any CD signals. In contrast to the behavior of *o*-**C**, however, even the addition of chiral guests *R*- or *S*-CSA did not lead to the appearance of cage-derived CD signals (Supporting Information Figure S38). Hence, the fixed stereochemistry of the closed-form DTE backbones is not affected by the presence of the chiral guest.

Enantiomeric Excess Determination. Subsequently, we examined whether the induced chirality of the open-form host–guest complexes [*R*-CSA@*o*-**C**] and [*S*-CSA@*o*-**C**] can be locked within the cage's DTE backbones upon irradiation with 313 nm light. First, we irradiated a CD_3CN solution of cage *o*-**C** containing 1.5 equiv of *R*-CSA or *S*-CSA at room temperature. The colorless [*R*/*S*-CSA@*o*-**C**] solution turned deep blue and a new UV absorption band was observed around 585 nm (Figure 5a and c and Supporting Information Figure S42). Completion of the photoreaction was monitored by ^{1}H NMR spectroscopy. The CD spectra showed a negative Cotton effect corresponding to the closed-form DTE chromophore for the sample containing *R*-CSA and a positive one for *S*-CSA, albeit of low intensity (Figure 5b and d and Supporting Information Figure S42). We explain this observation with a photochemical fixation of an enantiomeric excess in the form of the configurationally stable closed-form DTE isomers, induced by the presence of the chiral guest. Since we observed that the degree of chiral transfer within [*R*/*S*-CSA@*o*-**C**] apparently increases with decreasing temperature (Figure 4d), we tested the same procedure at several lower temperatures down to 77 K. Therefore, a quartz NMR tube containing the acetonitrile solution of [*R*/*S*-CSA@*o*-**C**] was immersed in different cooling baths in a transparent quartz dewar and irradiated with 313 nm light until full conversion of

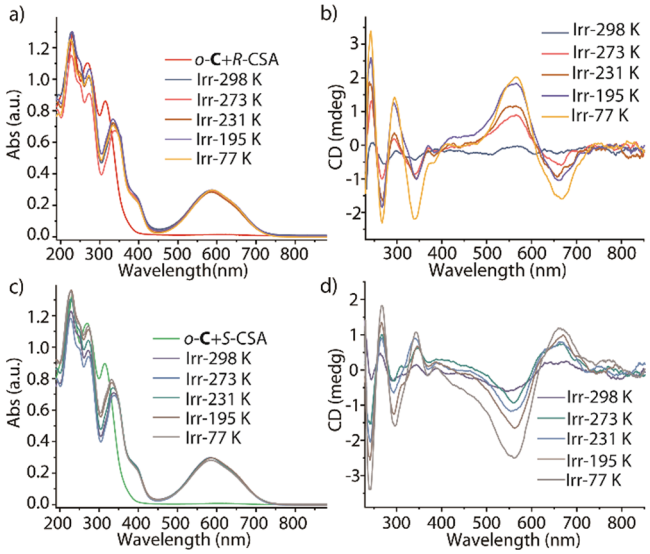

Figure 5. (a and c) UV–vis and (b and d) CD spectra of *o*-**C** (0.05 mM, CH_3CN) containing 1.5 equiv of *R*-CSA or *S*-CSA, respectively, after irradiation with 313 nm light at temperatures from 298 to 77 K (irradiation interval until complete conversion).

the photoreaction was achieved. Interestingly, the final ^{1}H NMR spectra of the fully photoisomerized cages revealed that the proton signals became sharper as the bath temperature decreased, indicating a reduction of the number of major diastereomeric components (Supporting Information Figure S40). In addition, the CD spectra showed increasing signal intensities with decreasing bath temperatures, indicating enrichment of one ligand enantiomer over the other (Figure 5b and d and Supporting Information Figure S42). We then disassembled the closed-form cages by adding aqueous NBu_4OH and ethylenediaminetetraacetic acid disodium salt (Na_2EDTA), followed by extraction with dichloromethane (DCM) under strict exclusion of light. The solution containing enriched ligands *R*,*R*-*c*-**L** and *S*,*S*-*c*-**L** was examined for enantiomeric excess (ee) by chiral HPLC. Table 1 summarizes

Table 1. Enantiomeric Excess (ee) of Ligands *S*,*S*-*c*-L and *R*,*R*-*c*-L after Irradiation of [*R*/*S*-CSA@o-C] with 313 nm Light at Various Temperatures (*R*-CSA Induces Enrichment of *S*,*S*-*c*-L)

ee (%)[a]	298 K	273 K[b]	231 K[c]	195 K[d]	77 K[e]
R-CSA	7	8	13	21	28
S-CSA	10	13	14	24	31

[a]Values determined by HPLC (monitored at 600 nm, estimated error ±5%) with a Chiralpak IA column. [b]Ice–water. [c]Dry ice–acetonitrile. [d]Dry ice–acetone. [e]Liquid nitrogen.

the results, showing that the enrichment improves at lower temperatures. The maximum obtained ee values were around 30 ± 5% for both guest enantiomers (considering HPLC signal integration difficulties due to signal overlap; see Supporting Information Table S1).

Evaluation of Guest Ejection Mechanism. On the basis of the observed degree of chiral induction as well as experiments described below, we assumed that the guest is ejected from the host early on, i.e., after the first DTE switch has been closed, during the stepwise ligand isomerization sequence (Figure 1b). Following this hypothesis, photo-

DOI: 10.1021/jacs.8b11872
J. Am. Chem. Soc. 2019, 141, 2097–2103

isomerization of the first ligand in *o*-**C** already results in a significant change of the structure and dynamics of the resulting cage $[Pd_2(o\text{-}\mathbf{L})_3(c\text{-}\mathbf{L})_1](BF_4)_4$ (=*m*-$\mathbf{C}^{3:1}$), bringing it close in shape to the fully switched isomer *c*-**C**. Like *c*-**C**, partially switched $[Pd_2(o\text{-}\mathbf{L})_3(c\text{-}\mathbf{L})_1](BF_4)_4$ would then be an inapt host for the CSA guest, leading to its ejection. Consequently, assuming a potent chirality transfer to all four ligands within [*R*-CSA@*o*-**C**] at the lowest studied temperatures, the guest's stereochemical information would remain locked only within the first switched DTE ligand, while the other three ligands would lose chiral information after guest excretion, followed by nonstereoselective photoisomerization. Hence, chiral information transfer onto one out of four ligands would explain ee values of around 25% for isolated *c*-**L**.

To test this hypothesis, we prepared cages from mixtures of *o*-**L** and *c*-**L** in different ratios. As thermodynamically controlled self-assembly thwarts the selective and exclusive synthesis of a single isomer (i.e., the one containing three open and one closed ligands), we had to base the following experiments on statistical mixtures of mixed-ligand cages. For a 3:1 mixture, ^{1}H NMR and ion mobility ESI mass spectra indicate the formation of a mixture of cage isomers containing the desired isomer $[Pd_2(o\text{-}\mathbf{L})_3(c\text{-}\mathbf{L})_1](BF_4)_4]$ (*m*-$\mathbf{C}^{3:1}$) as dominant species (~42%; besides ~32% *o*-**C**; see Supporting Information).

A first indication supporting that *m*-$\mathbf{C}^{3:1}$ closely resembles *c*-**C** came from a comparison of their DOSY NMR spectra, showing that the hydrodynamic radius of *m*-$\mathbf{C}^{3:1}$ is much closer to that of *c*-**C** than that of *o*-**C** (Supporting Information Figure S59). Furthermore, PM6- and DFT-calculated energy potentials obtained by squeezing *o*-**C**, *m*-$\mathbf{C}^{3:1}$, and *c*-**C** along their Pd−Pd axes indicated a major impact on cage conformational dynamics already induced by one closed ligand (Supporting Information Figure S66).

Second, we turned to chiral induction experiments using mixed-ligand cage samples *m*-$\mathbf{C}^{3:1}$, *m*-$\mathbf{C}^{2:2}$, and *m*-$\mathbf{C}^{1:3}$. When we examined the degree of chiral induction caused by addition of *R*/*S*-CSA to the mixed *m*-$\mathbf{C}^{3:1}$/*o*-**C** sample on the contained *o*-**L** chromophores, we observed that only the fraction of contained *o*-**C** (~32%) contributes to the characteristic CD signal at 330 nm, while the major species *m*-$\mathbf{C}^{3:1}$ does not (Supporting Information Figure S60). A systematic comparison of UV−vis and CD band intensities of *o*-**C**, *m*-$\mathbf{C}^{3:1}$, *m*-$\mathbf{C}^{2:2}$, *m*-$\mathbf{C}^{1:3}$, and *c*-**C** containing 1.5 equiv of *S*-CSA further clarified the situation: Whereas plotting the absorption maximum of *c*-**L** (585 nm) against the *o*-**L**/*c*-**L** ratio superimposes with the contained percentage of *c*-**L** (linear relationship), the plot of the observed guest-induced CD intensities in the same samples monitored at 330 nm (ellipticity maximum of *o*-**L**) against the *o*-**L**/*c*-**L** ratio nonlinearly follows the statistical content of *o*-**C** (Figures S61 and S62). Thus, chiral induction is only expressed in the contained fraction of *o*-**C** in all samples, not in $[Pd_2(o\text{-}\mathbf{L})_3(c\text{-}\mathbf{L})_1]$, $[Pd_2(o\text{-}\mathbf{L})_2(c\text{-}\mathbf{L})_2]$, $[Pd_2(o\text{-}\mathbf{L})_1(c\text{-}\mathbf{L})_3]$, or *c*-**C**, indicating that the guest cannot bind when at least one photoswitch is closed.

Third, we irradiated *m*-$\mathbf{C}^{3:1}$(*R*/*S*) (synthesized with 1 equiv of enantiomerically pure *R*,*R*- or *S*,*S*-c-**L**) under 313 nm at 231 K and found that the ee value remains around 29 ± 5% after cage disassembly, showing that *interligand* chirality transfer does not play any significant role (Supporting Information Table S5).

Fourth, irradiation of *m*-$\mathbf{C}^{3:1}$ (with racemic *c*-**L**) in the presence of 1.5 equiv of *R*-CSA or *S*-CSA gave ee values only around 8%, assumed to be caused by the contained 32% share of *o*-**C** alone (Supporting Information Table S5). All results detailed above agree with our hypothesis that only the first switching ligand effectively experiences the encapsulated guest's chirality, followed by guest ejection and photocyclization of the residual three ligands without stereocontrol.

Trapped Ion Mobility Mass Spectrometry. As a further orthogonal technique aimed at supporting the above stated mechanism, we employed trapped ion mobility spectroscopy (TIMS) coupled to ESI MS to obtain further insights into the structure of the host−guest aggregates (Figure 6). Results

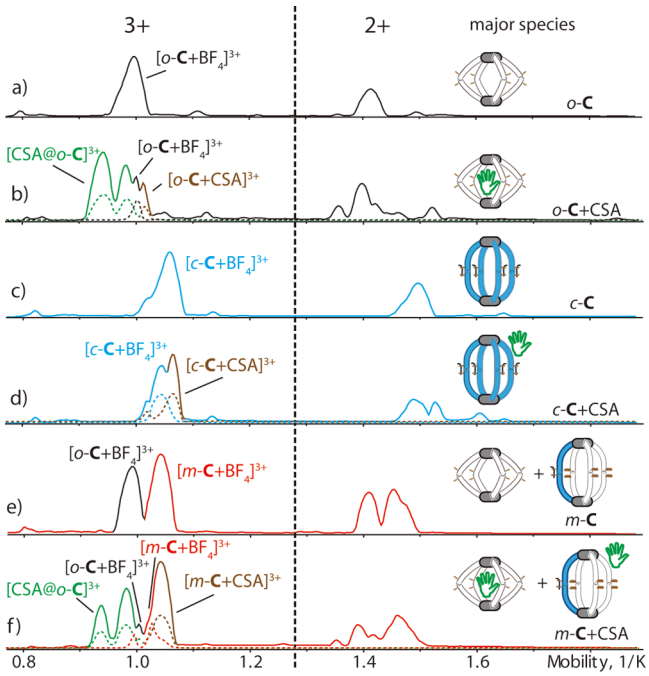

Figure 6. Ion mobility spectra of hosts (a) *o*-**C**; (c) *c*-**C**, and (e) *m*-**C** and corresponding samples containing 1.5 equiv of *R*-CSA: (b) *o*-**C** +*R*-CSA; (d) *c*-**C**+*R*-CSA, and (f) *m*-**C**+*R*-CSA.

show that the drift time (correlating with the collisional cross section; see Supporting Information Figure S65) of *o*-**C** (Figure 6a) is shorter than that of *c*-**C** (Figure 6c) and *m*-**C** (Figure 6e), while those of *c*-**C** and *m*-**C** are very close (all in accordance with the DOSY NMR results). After adding 1.5 equiv of *R*- or S-CSA, the mobilogram of *o*-**C** shows two extra signals (Figure 6b, fragment $[Pd(o\text{-}\mathbf{L})_2]^{2+}$ not counted), one with shorter drift time (smaller size) and a shoulder with longer drift time (larger size). Both signals correspond to the mass of the cage plus CSA, as seen in the mobility-filtered mass spectra. We assign the former signal to the host−guest complex CSA@*o*-**C** since encapsulation of the organic guest is expected to lead to a dispersion-driven compaction in the gas phase. In contrast, the signal with longer drift time is most likely attributed to an adduct with externally associated guest (*o*-**C** +CSA), leading to an overall size increase. When CSA is added to *c*-**C**, only one signal corresponding to the mass of cage plus CSA is observed, possessing a larger size than *c*-**C**, thus representing outside adduct *c*-**C**+CSA (Figure 6d), in full accordance with the above-described observation that *c*-**C** is not able to encapsulate the guest. For *m*-**C**, similarly to *c*-**C**, only a slight drift time increase was observed after add-

DOI: 10.1021/jacs.8b11872
J. Am. Chem. Soc. 2019, 141, 2097−2103

ing the guest (Figure 6f), indicating that both *m*-**C** and *c*-**C** show the same outside-aggregation behavior.

CONCLUSIONS

In conclusion, our study revealed the temporal relationship between the stepwise photocyclization events and guest ejection of a light-triggered host composed of four DTE photoswitches. We showed that encapsulation of a chiral guest inside the nonchiral, photochromic coordination cage *o*-**C** results in strong induced CD effects. Chiral information could be locked into the configurationally stable photoisomer *c*-**C** by UV irradiation. The degree of noncovalent propagation of chiral information was found to be dependent on temperature, guest amount, and absence of competing guests, but never exceeded about 25%. The latter observation, backed by a canon of NMR and CD experiments, X-ray, and ion mobility mass spectrometric studies, shows that already the closure of the first photoswitch triggers the key structural conversion that leads to ejection of the guest. The herein introduced methodology, based on chirality reporters lining the walls of a self-assembled confinement, serves as a basis for the examination of further host-to-guest size/shape relationships, including the role of solvent effects. Furthermore, progress in the fundamental understanding as well as application of chirality transfer will spur developments in the fields of enantioselective homogeneous catalysis, supramolecular recognition, and information processing on a molecular scale.

ASSOCIATED CONTENT

Supporting Information

The Supporting Information is available free of charge on the ACS Publications website at DOI: 10.1021/jacs.8b11872.

Synthetic procedures, NMR, MS, X-ray, and further spectroscopic data, DFT calculation results (PDF)

Crystallographic data (CIF)

Crystallographic data (CIF)

AUTHOR INFORMATION

Corresponding Author

*guido.clever@tu-dortmund.de

ORCID

Joakim Andréasson: 0000-0003-4695-7943

Guido H. Clever: 0000-0001-8458-3060

Notes

The authors declare no competing financial interest.

ACKNOWLEDGMENTS

This work was supported by the Deutsche Forschungsgemeinschft (DFG) under SFB 1073 (project B05), Cluster of Excellence RESOLV (EXC 1069), and GRK 2376 (331085229). Further support through ERC Consolidator grant RAMSES (683083) is acknowledged. Diffraction data for *o*-**C** were collected at PETRA III at DESY, a member of the Helmholtz Association (HGF). The authors thank Dr. Anja Burkhardt for assistance in using synchrotron beamline P11 (I-20160736). We thank Christiane Heitbrink, Andreas Brockmeyer, Dr. Petra Janning (MPI Dortmund), and Laura Schneider for measuring the ESI mass spectra as well as Kristian Surich, Alexandra Klauke, TUDO and RUB glass workshops for technical support. We thank Prof. Lars Schäfer, Prof. Patrick Nürnberger and Prof. Christian Merten (Ruhr University Bochum) for helpful discussions.

REFERENCES

(1) (a) McConnell, A. J.; Wood, C. S.; Neelakandan, P. P.; Nitschke, J. R. Stimuli-Responsive Metal−Ligand Assemblies. *Chem. Rev.* **2015**, *115*, 7729. (b) Xue, M.; Yang, Y.; Chi, X.; Yan, X.; Huang, F. Development of Pseudorotaxanes and Rotaxanes: From Synthesis to Stimuli-Responsive Motions to Applications. *Chem. Rev.* **2015**, *115*, 7398. (c) Jochum, F. D.; Theato, P. Temperature- and light-responsive smart polymer materials. *Chem. Soc. Rev.* **2013**, *42*, 7468. (d) Tam, A. Y.; Yam, V. W. Recent advances in metallogels. *Chem. Soc. Rev.* **2013**, *42*, 1540. (e) Doring, A.; Birnbaum, W.; Kuckling, D. Responsive hydrogels − structurally and dimensionally optimized smart frameworks for applications in catalysis, micro-system technology and material science. *Chem. Soc. Rev.* **2013**, *42*, 7391. (f) Klajn, R. Spiropyran-based dynamic materials. *Chem. Soc. Rev.* **2014**, *43*, 148. (g) Wang, W.; Wang, Y. X.; Yang, H. B. Supramolecular transformations within discrete coordination-driven supramolecular architectures. *Chem. Soc. Rev.* **2016**, *45*, 2656. (h) Jones, C. D.; Steed, J. W. Gels with sense: supramolecular materials that respond to heat, light and sound. *Chem. Soc. Rev.* **2016**, *45*, 6546. (i) Liu, Y.; Parks, F. C.; Zhao, W.; Flood, A. H. Sequence-controlled Stimuli-responsive Single-Double Helix Conversion between 1:1 and 2:2 Chloride-Foldamer Complexes. *J. Am. Chem. Soc.* **2018**, *140*, 15477. (j) Qi, Z.; Schalley, C. A.; Schneider, H.-J. Multi-stimuli Responsive Materials. In *Chemoresponsive Materials*; Schneider, H. J., Ed.; RSC Publishing, 2015. (k) Nobel Prize in Chemistry 2016: Stoddart, J. F. Mechanically Interlocked Molecules (MIMs) - Molecular Shuttles, Switches, and Machines. *Angew. Chem., Int. Ed.* **2017**, *56*, 11094. Sauvage, J.-P. From Chemical Topology to Molecular Machines. *Angew. Chem., Int. Ed.* **2017**, *56*, 11080. Feringa, B. L. The Art of Building Small: From Molecular Switches to Motors. *Angew. Chem., Int. Ed.* **2017**, *56*, 11060.

(2) (a) Wang, L.; Li, Q. Photochromism into nanosystems: towards lighting up the future nanoworld. *Chem. Soc. Rev.* **2018**, *47*, 1044. (b) Samanta, D.; Gemen, J.; Chu, Z.; Diskin-Posner, Y.; Shimon, L. J. W.; Klajn, R. Reversible photoswitching of encapsulated azobenzenes in water. *Proc. Natl. Acad. Sci. U. S. A.* **2018**, *115*, 9379. (c) Chen, S.; Chen, L. J.; Yang, H. B.; Tian, H.; Zhu, W. Light-Triggered Reversible Supramolecular Transformations of Multi-Bisthienylethene Hexagons. *J. Am. Chem. Soc.* **2012**, *134*, 13596. (d) Qu, D. H.; Wang, Q. C.; Zhang, Q. W.; Ma, X.; Tian, H. Photoresponsive Host−Guest Functional Systems. *Chem. Rev.* **2015**, *115*, 7543. (e) Diaz-Moscoso, A.; Ballester, P. Light-responsive molecular containers. *Chem. Commun.* **2017**, *53*, 4635. (f) Petermayer, C.; Dube, H. Indigoid Photoswitches: Visible Light Responsive Molecular Tools. *Acc. Chem. Res.* **2018**, *51*, 1153. (g) Mallo, N.; Foley, E. D.; Iranmanesh, H.; Kennedy, A. D. W.; Luis, E. T.; Ho, J.; Harper, J. B.; Beves, J. E. Structure−function relationships of donor−acceptor Stenhouse adduct photochromic switches. *Chem. Sci.* **2018**, *9*, 8242. (h) Banghart, M. R.; Mourot, A.; Fortin, D. L.; Yao, J. Z.; Kramer, R. H.; Trauner, D. Photochromic Blockers of Voltage-Gated Potassium Channels. *Angew. Chem., Int. Ed.* **2009**, *48*, 9097. (i) Dube, H.; Ajami, D.; Rebek, J., Jr. Photochemical Control of Reversible Encapsulation. *Angew. Chem., Int. Ed.* **2010**, *49*, 3192. (j) Park, J.; Sun, L. B.; Chen, Y. P.; Perry, Z.; Zhou, H. C. Azobenzene-Functionalized Metal−Organic Polyhedra for the Optically Responsive Capture and Release of Guest Molecules. *Angew. Chem., Int. Ed.* **2014**, *53*, 5842. (k) Wei, S. C.; Pan, M.; Fan, Y. Z.; Liu, H.; Zhang, J.; Su, C. Y. Creating Coordination-Based Cavities in a Multiresponsive Supramolecular Gel. *Chem. - Eur. J.* **2015**, *21*, 7418.

(3) (a) Yamamoto, H.; Carreira, E. M., Eds. *Comprehensive Chirality*, 1st ed.; Elsevier: Amsterdam, 2012. (b) Feringa, B. L.; van Delden, R. A. Absolute Asymmetric Synthesis: The Origin, Control, and Amplification of Chirality. *Angew. Chem., Int. Ed.* **1999**, *38*, 3418. (c) Palmans, A. R.; Meijer, E. W. Amplification of Chirality in Dynamic Supramolecular Aggregates. *Angew. Chem., Int. Ed.* **2007**, *46*,

DOI: 10.1021/jacs.8b11872
J. Am. Chem. Soc. 2019, 141, 2097−2103

8948. (d) Yoon, M.; Srirambalaji, R.; Kim, K. Homochiral Metal–Organic Frameworks for Asymmetric Heterogeneous Catalysis. *Chem. Rev.* **2012**, *112*, 1196. (e) Yang, C.; Inoue, Y. Supramolecular photochirogenesis. *Chem. Soc. Rev.* **2014**, *43*, 4123. (f) Hembury, G. A.; Borovkov, V. V.; Inoue, Y. Chirality-Sensing Supramolecular Systems. *Chem. Rev.* **2008**, *108*, 1.

(4) (a) Seeber, G.; Tiedemann, B. E. F.; Raymond, K. N. Supramolecular Chirality in Coordination Chemistry. *Top. Curr. Chem.* **2006**, *265*, 147. (b) Liu, M.; Zhang, L.; Wang, T. Supramolecular Chirality in Self-Assembled Systems. *Chem. Rev.* **2015**, *115*, 7304. (c) Raynal, M.; Ballester, P.; Vidal-Ferran, A.; van Leeuwen, P. W. N. M. Supramolecular catalysis. Part 1: non-covalent interactions as a tool for building and modifying homogeneous catalysts. *Chem. Soc. Rev.* **2014**, *43*, 1660. (d) Chen, L.-J.; Yang, H.-B.; Shionoya, M. Chiral metallosupramolecular architectures. *Chem. Soc. Rev.* **2017**, *46*, 2555. (e) Yan, K.; Dubey, R.; Arai, T.; Inokuma, Y.; Fujita, M. Chiral Crystalline Sponges for the Absolute Structure Determination of Chiral Guests. *J. Am. Chem. Soc.* **2017**, *139*, 11341. (f) Prins, L. J.; Timmerman, P.; Reinhoudt, D. N. Amplification of Chirality: The "Sergeants and Soldiers" Principle Applied to Dynamic Hydrogen-Bonded Assemblies. *J. Am. Chem. Soc.* **2001**, *123*, 10153.

(5) (a) Nishioka, Y.; Yamaguchi, T.; Kawano, M.; Fujita, M. Asymmetric [2 + 2] Olefin Cross Photoaddition in a Self-Assembled Host with Remote Chiral Auxiliaries. *J. Am. Chem. Soc.* **2008**, *130*, 8160. (b) Xuan, W.; Zhang, M.; Liu, Y.; Chen, Z.; Cui, Y. A Chiral Quadruple-Stranded Helicate Cage for Enantioselective Recognition and Separation. *J. Am. Chem. Soc.* **2012**, *134*, 6904. (c) Gütz, C.; Hovorka, R.; Klein, C.; Jiang, Q.; Bannwarth, C.; Engeser, M.; Schmuck, C.; Assenmacher, W.; Mader, W.; Topić, F.; Rissanen, K.; Grimme, S.; Lützen, A. Enantiomerically Pure $[M_6L_{12}]$ or $[M_{12}L_{24}]$ Polyhedra from Flexible Bis(Pyridine) Ligands. *Angew. Chem., Int. Ed.* **2014**, *53*, 1693. (d) Wang, X.; Wang, Y.; Yang, H.; Fang, H.; Chen, R.; Sun, Y.; Zheng, N.; Tan, K.; Lu, X.; Tian, Z.; Cao, X. Assembled molecular face-rotating polyhedra to transfer chirality from two to three dimensions. *Nat. Commun.* **2016**, *7*, 12469. (e) Sun, J.; Bennett, J. L.; Emge, T. J.; Warmuth, R. Thermodynamically Controlled Synthesis of a Chiral Tetra-cavitand Nanocapsule and Mechanism of Enantiomerization. *J. Am. Chem. Soc.* **2011**, *133*, 3268.

(6) Castilla, A. M.; Ousaka, N.; Bilbeisi, R. A.; Valeri, E.; Ronson, T. K.; Nitschke, J. R. High-Fidelity Stereochemical Memory in a FeII4L4 Tetrahedral Capsule. *J. Am. Chem. Soc.* **2013**, *135*, 17999.

(7) Rivera, J. M.; Martín, T.; Rebek, J. Chiral Spaces: Dissymmetric Capsules Through Self-Assembly. *Science* **1998**, *279*, 1021.

(8) (a) Terpin, A. J.; Ziegler, M.; Johnson, D. W.; Raymond, K. N. Resolution and Kinetic Stability of a Chiral Supramolecular Assembly Made of Labile Components. *Angew. Chem., Int. Ed.* **2001**, *40*, 157. (b) Davis, A. V.; Fiedler, D.; Ziegler, M.; Terpin, A.; Raymond, K. N. Resolution of Chiral, Tetrahedral M4L6Metal–Ligand Hosts. *J. Am. Chem. Soc.* **2007**, *129*, 15354.

(9) (a) Irie, M.; Fukaminato, T.; Matsuda, K.; Kobatake, S. Photochromism of Diarylethene Molecules and Crystals: Memories, Switches, and Actuators. *Chem. Rev.* **2014**, *114*, 12174. (b) Zhang, J.; Tian, H. The Endeavor of Diarylethenes: New Structures, High Performance, and Bright Future. *Adv. Opt. Mater.* **2018**, *6*, 1701278.

(10) (a) Morimoto, M.; Kobatake, S.; Irie, M. Absolute asymmetric photocyclization in chiral diarylethene co-crystals with octafluoronaphthalene. *Chem. Commun.* **2008**, 335. (b) Kawamura, K.; Osawa, K.; Watanobe, Y.; Saeki, Y.; Maruyama, N.; Yokoyama, Y. Photocyclization of photoswitches with high enantioselectivity in human serum albumin in an artificial environment. *Chem. Commun.* **2017**, *53*, 3181.

(11) de Jong, J. J. D.; Lucas, L. N.; Kellogg, R. M.; van Esch, J. H.; Feringa, B. L. Reversible Optical Transcription of Supramolecular Chirality into Molecular Chirality. *Science* **2004**, *304*, 278.

(12) Pace, T. C.; Muller, V.; Li, S.; Lincoln, P.; Andreasson, J. Enantioselective Cyclization of Photochromic Dithienylethenes Bound to DNA. *Angew. Chem., Int. Ed.* **2013**, *52*, 4393.

(13) (a) Seidel, S. R.; Stang, P. J. High-Symmetry Coordination Cages via Self-Assembly. *Acc. Chem. Res.* **2002**, *35*, 972. (b) Cook, T. R.; Zheng, Y.-R.; Stang, P. J. Metal–Organic Frameworks and Self-Assembled Supramolecular Coordination Complexes: Comparing and Contrasting the Design, Synthesis, and Functionality of Metal–Organic Materials. *Chem. Rev.* **2013**, *113*, 734. (c) Smulders, M. M. J.; Riddell, I. A.; Browne, C.; Nitschke, J. R. Building on architectural principles for three-dimensional metallosupramolecular construction. *Chem. Soc. Rev.* **2013**, *42*, 1728.

(14) (a) Han, M.; Engelhard, D. M.; Clever, G. H. Self-assembled coordination cages based on banana-shaped ligands. *Chem. Soc. Rev.* **2014**, *43*, 1848. (b) Clever, G. H.; Punt, P. Cation–Anion Arrangement Patterns in Self-Assembled Pd2L4 and Pd4L8 Coordination Cages. *Acc. Chem. Res.* **2017**, *50*, 2233.

(15) (a) Han, M.; Michel, R.; He, B.; Chen, Y.-S.; Stalke, D.; John, M.; Clever, G. H. Light-Triggered Guest Uptake and Release by a Photochromic Coordination Cage. *Angew. Chem., Int. Ed.* **2013**, *52*, 1319. (b) Han, M.; Luo, Y.; Damaschke, B.; Gomez, L.; Ribas, X.; Jose, A.; Peretzki, P.; Seibt, M.; Clever, G. H. Light-Controlled Interconversion between a Self-Assembled Triangle and a Rhombicuboctahedral Sphere. *Angew. Chem., Int. Ed.* **2016**, *55*, 445.

(16) (a) Wiedbrauk, S.; Bartelmann, T.; Thumser, S.; Mayer, P.; Dube, H. Simultaneous complementary photoswitching of hemithioindigo tweezers for dynamic guest relocalization. *Nat. Commun.* **2018**, *9*, 1456. (b) Hua, Y.; Flood, A. H. Flipping the Switch on Chloride Concentrations with a Light-Active Foldamer. *J. Am. Chem. Soc.* **2010**, *132*, 12838. (c) Diaz-Moscoso, A.; Arroyave, F. A.; Ballester, P. Moving systems of polar dimeric capsules out of thermal equilibrium by light irradiation. *Chem. Commun.* **2016**, *52*, 3046.

DOI: 10.1021/jacs.8b11872
J. Am. Chem. Soc. 2019, 141, 2097–2103